Journal of Thermal Analysis and Calorimetry (2018) 133:189–197
https://doi.org/10.1007/s10973-018-7031-3

About thermostability of biocompatible Ti–Zr–Ag–Pd–Sn amorphous alloys

Mircea Nicoara[1] · Dragos Buzdugan[1] · Cosmin Locovei[1] · Traian Bena[1] · Mihai Stoica[1,2]

Received: 14 August 2017 / Accepted: 21 January 2018 / Published online: 29 January 2018

Abstract
A new Ti-based amorphous alloy without any harmful additions of elements and supplementary Ag content was developed for applications in orthopedics and dentistry. Since complete elimination of toxic elements is reducing the glass-forming ability and direct casting of massive components is no longer possible, the new alloy was produced by melt spinning as thin ribbons, which could be subsequently processed by powder metallurgy. Investigations of X-ray diffraction and high-resolution transmission electron microscopy evidenced the fully amorphous structure of the new alloy. Differential scanning calorimetry was used to determine the crystallization point and the heating behavior at rates between 5 and 30 K min^{-1} in order to estimate by Kissinger's method the activation energy for crystallization. Investigations evidence that the new $Ti_{30}Zr_{32}Ag_7Pd_{24}Sn_7$ crystallizes at around 500 °C and the value of activation energy is relatively low in comparison with similar Ti-based alloys that were successfully processed by powder metallurgy; therefore, thermomechanical processing should be performed exclusively below 500 °C during short fabrication cycles, in order to preserve the amorphous structure.

Keywords Ti-based amorphous alloys · Biocompatible materials · Melt spinning · Kissinger's method · Thermostability

Introduction

Titanium alloys still represent the standard solution for implants used in dentistry and orthopedics, mostly because of their appropriate mechanical properties and high corrosion resistance. In fact, the Ti-based biomaterials surpass the polymers in terms of mechanical strength, while their better toughness and fatigue strength make them a much safer choice in comparison with the advanced bioceramics [1–4].

Although titanium alloys are the most popular biomaterials some of their drawbacks became obvious over the years. Among the four major causes for the failure of orthopedic implants, which are wear/corrosion, fibrous encapsulation, inflammation/rejection, low toughness/fatigue strength and rigidity mismatch with the bone [1], most of them could be related to the imperfections of titanium alloys that are currently in use. For example, low wear resistance and mediocre corrosion stability produce debris that could go to blood producing toxic effects, while fibrous encapsulation and inflammations are considered to be caused by the metallic ions of the alloying elements that are released in the human body. High mechanical strength that could be achieved by complex alloying will result also in a much higher rigidity than human bone. The effect of stress shielding is rather high, since, for example, the Ti–6Al–4V alloy has a Young's modulus of about 112 GPa, making it significantly more rigid than the cortical bone, which could have between 4 and 30 GPa [2, 3, 5].

An interesting development of titanium alloys was achieved with the development of massive amorphous components (i.e., critical dimensions more than 1 mm), also called bulk metallic glasses (BMGs), and usually produced by means of ultra-rapid cooling. Their mechanical properties are characterized by a higher ratio between mechanical strength and rigidity, which improves the biomechanical behavior of implants [6–10]. Corrosion resistance is also considerably enhanced, since amorphous

✉ Mircea Nicoara
mircea.nicoara@upt.ro

[1] Politehnica University Timisoara, 300222 Timisoara, Romania

[2] ETH Zürich, 8093 Zurich, Switzerland

alloys have no dislocations or grain limits and show better microstructural homogeneity, providing therefore an improved biocompatibility. However, fabrication of large-sized BMGs involves alloying with some amorphization elements that have cytotoxic effects, like Cu, Zn and Be, or may be responsible for other harmful consequences, like Ni, Co, Cr, Fe, Mo, V, Al and Mn [5, 11–13]. Consequently, fabrication of large-sized BMGs with acceptable biocompatibility remains problematic.

Recent researches are focused on some new directions that could be promising for the development of titanium alloys. Since Ti-based BMGs are usually characterized by extreme fragility, an interesting alternative is represented by composites with amorphous matrix reinforced by secondary phases, which could be crystalline, quasi-crystalline or amorphous and therefore provide better ductility [7, 14]. Production of such composites by means of ultra-rapid cooling may require only low amorphization capacity, and therefore, elements with better biocompatibility could be used for alloying of titanium.

Another interesting research direction with certain potential is represented by the fabrication by means of melt rapid cooling of amorphous powders or ribbons, which are subsequently processed through powder metallurgy. This approach could have two major advantages: production of powders or ribbons requires only biocompatible additions with low glass-forming ability (GFA), such as In, Nb, Pd, Si, Sn, Ta, Zr [9, 15–18], while processing via powder metallurgy allows achievement of controlled porosity, which may reduce the rigidity of titanium implants. These new porous materials, also called bulk metallic glass foams (BMGFs), could provide better biomechanical compatibility with human bone and stimulate cell migration and bone growth through interconnected pores, while the superficial porosity improves fixation by means of an increased interface between implant and bone [19–23].

Consolidation by way of sintering rises, however, an important structural problem, since amorphous state should be preserved during the heat treatment, without any significant crystallization. Therefore, the thermal stability of newly formulated alloys is of utmost importance, in terms of activation energy and crystallization temperature.

The current experiments are aiming to continue some previous researches of the authors for the replacement of harmful alloying elements like Ni and Cu with biocompatible elements like Ga, Si, Ta, Zr or Ag for the fabrication of amorphous/crystalline composite by means of ultra-rapid melt cooling [24, 25] or for the development of BMGFs using powder metallurgy processing of amorphous ribbons [26, 27].

The main contribution of the present research is the development of new amorphous Ti-based alloys to replace the Cu with Ag in the compositions of Ti–Zr–Cu–Pd alloying system. Although the Ti–Zr–Cu–Pd alloys with minor additions of other elements prove to be successful in casting rods with diameters of at least 4 mm [28], the presence of Cu as a very important amorphization element is problematic, considering its multiple toxic effects to the human body. The cytotoxic effect of Cu is already well established [11, 12], since it could inhibit bone regeneration, causing implant failure, while some reports also indicate possible genotoxic effects [29]. Regarding the use of Ag as amorphization element, a literature review may allow to conclude that cytotoxicity or other adverse effects of Ag are considerably lower [11, 30, 31]. Moreover, implants with Ag additions could benefit from its antimicrobial and antibacterial effects [32–34], with the condition of in vivo assessment of biocompatibility for the newly developed alloys. A more comprehensive study about the biologic effects of Cu and Ag could be found in our previous works [25, 26].

Materials and methods

Alloy design

The composition of the new Cu-free alloy is calculated based on the so-called orbital method developed by Morinaga [35, 36]. This method of alloy design uses two electronic parameters of chemical elements that compose a certain alloy, i.e., the bond order (*Bo*) and the d-orbital energy level of the metallic element (*Md*), which are calculated for a specific alloy with the following relations:

$$\bar{B}_{\mathrm{o}} = \sum_{i=1}^{n} x_{\mathrm{i}} (B_{\mathrm{o}})_{\mathrm{i}} \tag{1}$$

$$\bar{M}_{\mathrm{d}} = \sum_{i=1}^{n} x_{\mathrm{i}} (M_{\mathrm{d}})_{\mathrm{i}} \tag{2}$$

In relations (1) and (2) the electronic parameters of composing elements $(Bo)_{\mathrm{i}}$ and $(Md)_{\mathrm{i}}$ are taken from Table 1, while x_{i} represents the atomic proportion of each element. The calculated parameters of the new alloy $\bar{B}_{\mathrm{o}}$ and $\bar{M}_{\mathrm{d}}$ give the position on a special chart (Fig. 1) estimating

Table 1 Values of parameters *Bo* and *Md* for alloying elements in bcc. Ti, after [35]

Element	*Bo*	*Md*/eV
Ti	2.790	2.447
Zr	3.086	2.934
Pd	2.208	0.387
Cu	2.114	0.567
Ag	2.094	0.196
Sn	2.283	2.100
Nb	3.099	2.424

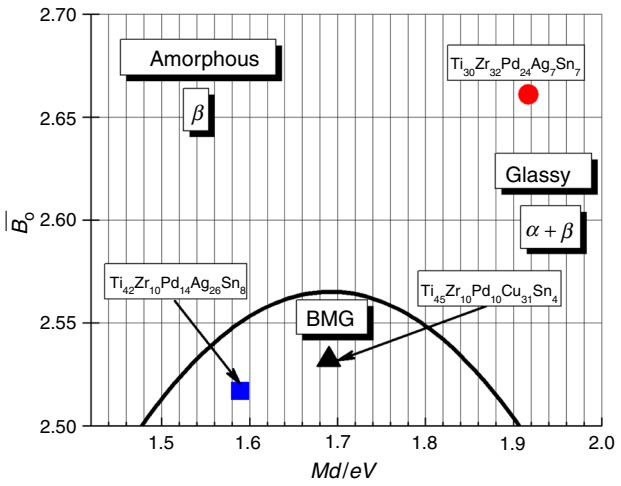

Fig. 1 Positions of the Cu-free $Ti_{42}Zr_{10}Pd_{14}Ag_{26}Sn_8$ and $Ti_{42}Zr_{10}Pd_{14}Ag_{26}Sn_8$ alloys, as well as the original $Ti_{45}Zr_{10}Pd_{10}Cu_{31}Sn_4$ alloy, on the chart of amorphous and glassy alloys, based on *Bo* and *Md* parameters, after [36]

its structural character: amorphous, glassy or bulk metallic glass (BMG).

Although the Morinaga's method proved to be precise in many situations, it should be considered with precaution. For example, previous experiments [25] were based on the estimation that a newly developed Cu-free alloy $Ti_{42}Zr_{10}Pd_{14}Ag_{26}Sn_8$, which resulted from the replacement of Cu in the already classical $Ti_{45}Zr_{10}Pd_{10}Cu_{31}Sn_4$, will be a bulk metallic glass. Although the prediction for $Ti_{45}Zr_{10}Pd_{10}Cu_{31}Sn_4$ was accurate, since 4-mm amorphous rods were fabricated successfully [28], in the case of $Ti_{42}Zr_{10}Pd_{14}Ag_{26}Sn_8$ fabricated by means of suction casting, some early separations of silver were evidenced, resulting a composite amorphous–crystalline structure. Preliminary experiments proved that silver separations could be prevented only if the Ag content was lower, and therefore, the final composition of the new Cu-free alloy was determined to be $Ti_{30}Zr_{32}Ag_7Pd_{24}Sn_7$ (Table 2).

The orbital method estimates that the $Ti_{30}Zr_{32}Ag_7Pd_{24}Sn_7$ is outside the BMG zone (Fig. 1), and the prediction proves to be correct, since massive rods fabricated by suctions casting contained crystalline fractions. Consequently, because the new $Ti_{30}Zr_{32}Ag_7Pd_{24}Sn_7$ seems to have a lower amorphization capacity than the Ti–Zr–Cu–Pd alloys, and only thin components could be fully amorphized, the best technological approach is casting of ribbons by means of melt spinning, which are subsequently processed by powder metallurgy. This fabrication route was successfully used by the authors for the development of a new amorphous $Ti_{42}Zr_{40}Ta_3Si_{15}$ alloy, completely free of any harmful elements, and will be therefore considered for the processing of the newly developed alloy. In that case, the resulting $Ti_{42}Zr_{40}Ta_3Si_{15}$ amorphous ribbons were fragmented to powder and subsequently consolidated by hot pressing. Fabrication of amorphous powder was performed using cryo-milling, considering the ductile behavior of ribbons, which were cut into small pieces, and then ball-milled under argon atmosphere in a planetary mill (Retsch PM400), using hardened steel balls and vials at 300 rpm, and a ball-to-powder weight ratio of about 10:1. The vials were immersed in liquid nitrogen for 15 min and then immediately milled for another 15 min. The cycle was repeated four times for a total milling time of 1 h. Before consolidation, the resulting powders were sieved to below 300 μm. The material was handled in a glove box under purified argon atmosphere (less than 0.1 ppm O_2 and H_2O) to avoid any possible contaminations. Hot pressing was performed using an automatic hydraulic system provided by Huttinger/Weber-Pressen, which allowed continuous pressure control. Some small disks 10 mm in diameter and about 3 mm thick were produced in a double-action pressing die, heated by induction, under argon gas protection, and each pressing operation was performed after thoroughly vacuum-degassing at 823 K for 3 min with a compaction pressure of 900 MPa. The final massive alloy has a mechanical strength of 337 MPa with a strain of 0.67%. Most remarkably, the porosity is around 14 vol%, which brings the apparent Young's modulus at only 52 GPa, much closer to the human bone, since similar Ti alloys have values of about 80-90 GPa [28, 37]. Details of the technology and resulting properties could be found elsewhere [26].

Experimental

The new Cu-free $Ti_{30}Zr_{32}Ag_7Pd_{24}Sn_7$ alloy was produced in the form of thin ribbons that could be further processed to massive components via powder metallurgy, as described in "Alloy design" section. Ribbons fabrication was performed in a two-stage processing route. Initially, a master alloy with the atomic percentage $Ti_{30}Zr_{32}Ag_7Pd_{24}Sn_7$ was prepared by arc melting using elements of purity

Table 2 Compositions and electronic parameters of Ti-based alloys

Alloy	Ti/at.%	Zr/at.%	Pd/at.%	Cu/at.%	Ag/at.%	Sn/at.%	*Bo*	*Md*/eV
$Ti_{30}Zr_{32}Pd_{24}Ag_7Sn_7$	30	32	24	–	7	7	2.661	1.917
$Ti_{42}Zr_{10}Pd_{14}Ag_{26}Sn_8$	42	10	14	–	26	8	2.517	1.589
$Ti_{45}Zr_{10}Pd_{10}Cu_{31}Sn_4$	45	10	10	31	–	4	2.532	1.689

higher than 99.9 wt%. High-purity argon was used as protection atmosphere, and a titanium getter provided additional cleaning of the protective gas. The master ingot was melted and flipped repeatedly for homogenization, which was relatively difficult to achieve, considering the differences between elements in terms of densities and melting points.

The melt spinning technique was subsequently adopted for fabrication of thin ribbons, since the GFA of the designed alloy seems to be too low for fabrication via ultra-rapid cooling of massive components with completely amorphous structure, and the resulting material is usually an amorphous/crystalline composite. The $Ti_{30}Zr_{32}Ag_7Pd_{24}Sn_7$ ribbons were produced on a single-roller Bühler melt spinner, at a circumferential speed of 35 ms^{-1}, using an ejection relative pressure of 400 mbar, the melt being previously overheated at $T = 1823$ K. Melt ejection was performed through a 1-mm orifice, and the distance between wheel and crucible was maintained at 1.2 mm. Resulting ribbons were continuous, about 40 μm thick and 5 mm wide.

Thermal properties of $Ti_{30}Zr_{32}Ag_7Pd_{24}Sn_7$ ribbons were determined by differential scanning calorimetry (DSC) on 20-mg samples under argon gas using a Netzsch STA 449F1 differential scanning calorimeter. The samples were heated in standard Al_2O_3 DSC/TG pans with lids, at heating rates of 5, 10, 15 and 30 °C min^{-1}, with alumina as reference material.

The structural character of amorphous ribbons was determined by means of X-ray diffraction (XRD) in Bragg–Brentano configuration, in continuous scanning mode using a step size of 0.0130° and 80-s step time, at room temperature. The XRD analysis was performed on a FEI X'Pert PRO MPD diffractometer with a copper anode X-ray tube having $\lambda = 0.155$ nm, PixCEL detector, vertical θ–θ goniometer and spinning sample holder.

The structure of the starting ribbons was further investigated by scanning electron microscopy (SEM) using a FEI Quanta 250 FEG scanning electronic microscope, and in high-resolution transmission electron microscopy (HR-TEM) on a FEI Tecnai G2 200 kV S/TEM microscope at 200 kV accelerating voltage. A FEI Quanta 3D dual-beam microscope using focused beams of gallium ions is used to prepare the TEM samples.

Theoretical considerations

The $Ti_{30}Zr_{32}Ag_7Pd_{24}Sn_7$ ribbons that were produced by means of an ultra-rapid cooling technique are characterized by metastable structures, which usually have higher internal energy than the crystalline phases. Such structures tend to reduce their free energy at heating, and resulting transformations typically contain two different stages. Initially, if heating is below the crystallization temperature, a reduction in the free energy will occur, accompanied with very complex processes of structural relaxation, which could result in changes in properties, such as ductility, hardness, specific volume and specific heat. The second stage of heating at temperatures above crystallization point consists in crystallizations produced by some polymorphous reactions, without changes in chemical composition [38].

Since the main objective of the research program consists in fabrication of massive amorphous components that should benefit from the valuable properties of BMG, processing route by means of powder metallurgy should not be accompanied by any crystallization, especially during consolidation by sintering. Therefore, the thermal stability of the new metallic glasses should be evaluated in terms of crystallization temperature and activation energy for crystallization. These values should be compared with those determined on similar amorphous materials that are appropriate for powder metallurgy processing.

Regarding the calculation of activation energy E_a [J mol^{-1}] for the crystallization of metallic glasses, the most commonly used is the Kissinger's relation [39–44], which is easily applicable to non-isothermal DSC experiments:

$$\ln\left(\frac{T_v^2}{V_i}\right) = \frac{E_a}{RT_v} + A \tag{3}$$

In relation (3) the symbols have the following meanings: T_v [K]—temperature point corresponding to the maximum crystallization rate, which corresponds to the maximum of the peak representing the exothermal reaction on the DSC thermograms, V_i [K s^{-1}]—heating rate used to determine the DSC curve, R [J mol^{-1} K^{-1}]—universal constant of gases, A—constant specific to analyzed material [45, 46]. For a set of isochronal experiments with different heating rates, the activation energy for crystallization E_a of a certain phase could be determined based on Eq. (3) from the slope of the plot determined by the parameters of experimental curves represented in the following coordinates:

$$\ln\left(\frac{T_v^2}{V_i}\right) = F\left(\frac{1}{T_v}\right). \tag{4}$$

Results and discussion

Considering the importance of accomplishing a fully amorphous state for the $Ti_{30}Zr_{32}Ag_7Pd_{24}Sn_7$ ribbons, special attention was given to XRD and TEM investigations to rule out the presence of any crystalline phases.

In this respect, Fig. 2 presents the XRD patterns that were determined on both wheel side and air side surface of the ribbons. Since resulting XRD patterns show no sharp peak reflections and the spectra are diffuse, typical to randomly ordered atoms, on both sides of the ribbons, it may be concluded with no doubt that the $Ti_{30}Zr_{32}Ag_7Pd_{24}Sn_7$ ribbons are fully amorphous.

Structural investigations by means of SEM reveal the homogeneous and fragile appearance of a fracture cross section of a melt-spun ribbon (the dark area in Fig. 3a), while the air side surface (light gray surface in Fig. 3b) seems to be relatively smooth. The amorphous character of the newly designed alloy is confirmed by HR-TEM image of the ribbon (Fig. 3b), which evidences only random distributions of atoms. The 2D selected area electron diffraction (SAED) pattern is characterized by a diffuse halo ring that is also typical to amorphous structure, confirming once again the results of XRD analysis.

The DSC investigations revealed a very complex configuration of the curves for heating, which was performed on constant rates of 5, 10, 15 and 30 °C min^{-1}. The DSC curve for 10 °C min^{-1} is shown in Fig. 4 and evidences some endothermic events with the onset at about 337 °C, which may be associated with the glass transition. However, the exact glass transition temperature remains difficult to determine, since the reaction is weak, which is in accordance with conclusions drawn by other authors who studied similar compositions [17]. Moreover, some marginal glass formers do not exhibit any glass transition at all [38]. At higher temperature, samples crystallize through several strong exothermic peaks, indicating formation of multiple crystalline phases, the first crystallization peak

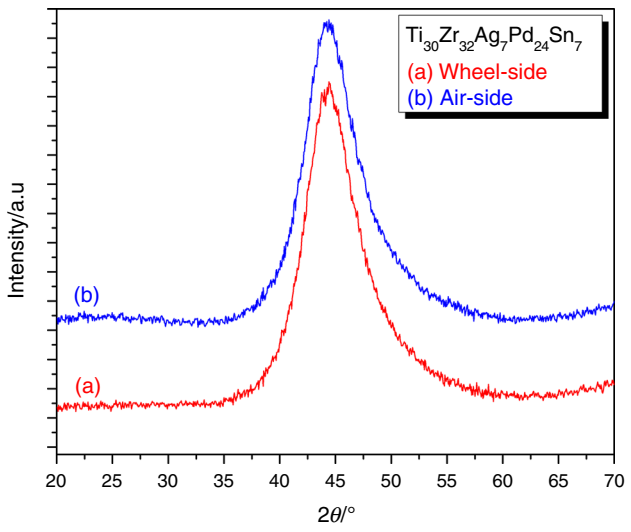

Fig. 2 XRD patterns for $Ti_{30}Zr_{32}Ag_7Pd_{24}Sn_7$ glassy alloy on both ribbon surfaces: (a) wheel side and (b) air side. The patterns are typical for completely amorphous alloys

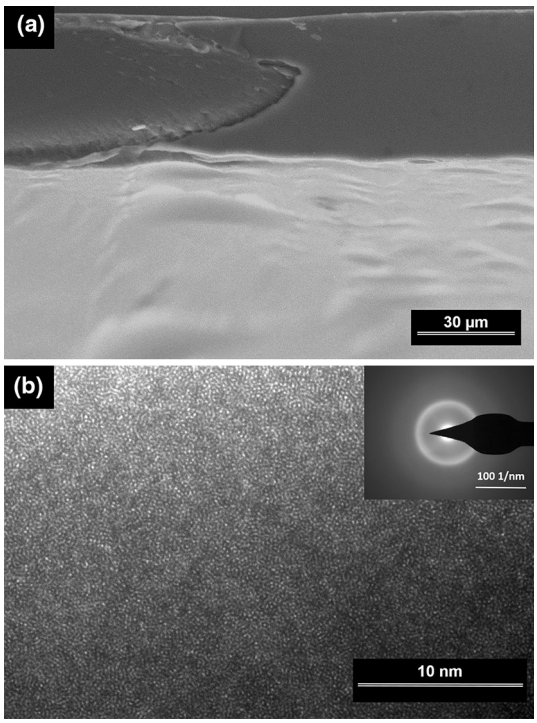

Fig. 3 Structural investigations on cast amorphous ribbons. **a** SEM micrograph showing the cross-sectional fracture (dark area) and the air side surface (light gray surface). **b** HR-TEM image with the inset of corresponding SAED pattern

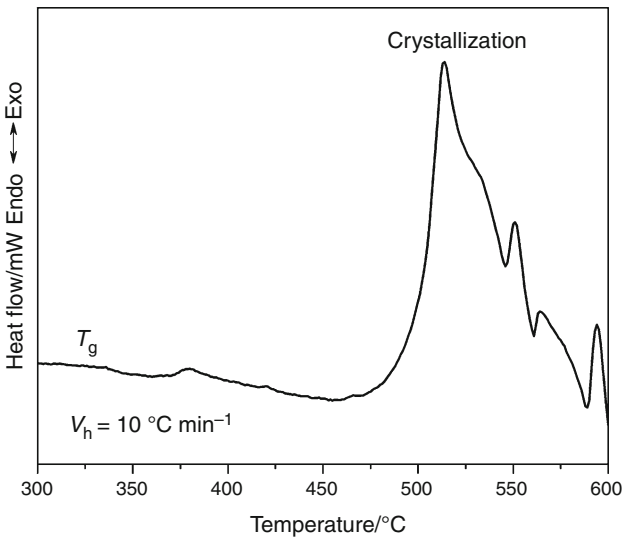

Fig. 4 DSC curve for $Ti_{30}Zr_{32}Ag_7Pd_{24}Sn_7$ amorphous ribbon at a heating rate of 10 °C min^{-1}

having the onset at $T_x = 499$ °C and the maximum at $T_v = 513$ °C.

Stability of the amorphous structures is evaluated by the activation energy necessary for crystallization of the phase that forms at the lowest point, represented by the first peak, which is usually responsible for the dramatic alteration of

properties. Therefore, to calculate the activation energy after Kissinger's relation, heating of samples was performed at several rates, i.e., 5, 10, 15 and 30 °C min^{-1}, in order to determine the peak of the first exothermic reaction T_v, as seen in Fig. 5. As the heating rate increases, glass transitions were even more faded and difficult to determine; however, the exothermic peaks that are of first importance for further analyses were evident.

Reaction kinetics usually determine formation of crystalline entities from amorphous phase with different rates through nucleation and growth. Since both events are temperature-dependent, the rates at which they occur are easily to determine following isothermal experiments. The formation of crystalline entities usually proceeds with different rates, according to the reaction kinetics. In the case of isochronal DSC measurements, which are easier to perform, it is largely considered that the maximum crystallization rate would correspond to the temperature of the exothermic peak [38] that is marked as T_v in Fig. 5. The experimentally determined peak temperatures T_v for all heating rates, which were further used for calculation of Kissinger's plot, are summarized in Table 3.

Figure 6 shows the representation of Kissinger's plot, which actually consists in a linear regression fitting of the points calculated for each heating rate with relation (4). The activation energy for first crystallization of the $Ti_{30}Zr_{32}Ag_7Pd_{24}Sn_7$ amorphous alloy is $E_a = 157$ kJ mol^{-1} and results as numerical equivalent to the slope of the line multiplied by the universal gas constant R.

It may be concluded that the activation energy of amorphous $Ti_{30}Zr_{32}Ag_7Pd_{24}Sn_7$ is considerably lower than the value determined in our previous researches for

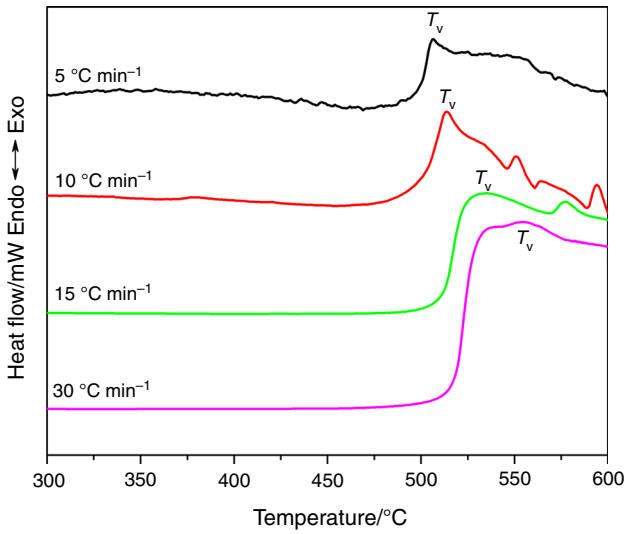

Fig. 5 The DSC curves measured for different heating rates. Maximum temperatures of the first peak T_v are further considered for Kissinger's calculation

Table 3 Peak of the first exothermic peak of DSC heating curves

No.	Heating rate V_h/°C min^{-1}	Tip of the peak T_v/°C
1	5	506
2	10	513
3	15	536
4	30	556

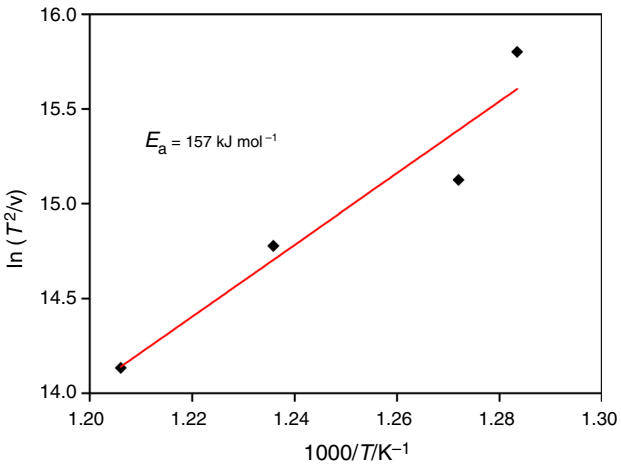

Fig. 6 Kissinger's plot of $Ti_{30}Zr_{32}Ag_7Pd_{24}Sn_7$ amorphous alloy

$Ti_{42}Zr_{40}Ta_3Si_{15}$, which had an activation energy $E_a = 310$ kJ mol^{-1} [27]. This exceptionally high value of activation energy attracted some attention, since higher crystallization stability facilitated the conservation of amorphous character during subsequent milling and hot pressing at 550 °C for 3 min, the final microstructure and mechanical properties being rather promising for applications as orthopedic implants [26]. Moreover, the peak of first crystallization for the new alloy is in proximity of 500 °C for the low heating rates, while crystallization of $Ti_{42}Zr_{40}Ta_3Si_{15}$ is almost 100 °C higher. However, the new $Ti_{30}Zr_{32}Ag_7Pd_{24}Sn_7$ alloy has an activation energy close to other similar alloys. For example, the basic amorphous $Ti_{41}Zr_{25}Be_{34}$ has an activation energy of crystallization of 181.3 kJ mol^{-1}, which increases with addition of Cu, Al, Cr, V, Ag up to the highest activation energy of 242.5 kJ mol^{-1}, while some other elements like Ni and Fe have the opposite effect. The main reason for these dramatic changes is that the initial $Ti_{41}Zr_{25}Be_{34}$ alloy normally crystallizes in α-Ti_2Zr, Be_2Zr and α-Ti phases, while alloying with elements like Fe, V, Cr results in formation of β-Ti, or some undetermined phases when Cu and Ni are added [47]. An illustration of the very complex effect of alloying elements is that Ni is considerable increasing thermal stability of $Ti_{41}Zr_{25}Be_{34}$, while partial replacement of Cu with Ni in amorphous $Ti_{50}Cu_{50}$ alloy increases the

activation energy, calculated after Kissinger, from 207 to 406 kJ mol^{-1} in the resulting $Ti_{50}Ni_{30}Cu_{20}$. [48].

A comparison with an intensively studied BMG like $Ti_{40}Zr_{10}Cu_{36}Pd_{14}$, which has the activation energy determined with the Kissinger's method of 287.6 kJ mol^{-1} and is considered to have high thermal stability to crystallization [49], reveals that the newly developed $Ti_{30}Zr_{32}Ag_7Pd_{24}Sn_7$ seems to be rather sensitive to heating. A literature review suggests that an important reason for that could be the replacement of Cu, which has the important effect of both increasing the GFA and the thermal stability of Ti-based amorphous alloys. For example 7 at.% of Cu added to the $Ti_{41}Zr_{25}Be_{28}Fe_6$ BMG will increase the activation energy of the crystallization, from 179 to 188 kJ mol^{-1}. The addition of Cu will also change the crystallization kinetics, since the basic $Ti_{41}Zr_{25}Be_{28}Fe_6$ alloy has only two exothermic reactions of crystallization, while modified $(Ti_{41}Zr_{25}Be_{28}Fe_6)_{93}Cu_7$ has four peaks. Multiple peaks are considered to reduce the nucleation and growth rate, which impede atomic diffusion and increase the GFA [50].

Another chemical element from the newly design composition is Sn, which seems to have stabilizing effects. The activation energy of amorphous $Ti_{41.5}Zr_{2.5}Hf_5Cu_{37.5}Ni_{7.5}Si_1Sn_5$ calculated after Kissinger is 409.51 kJ mol^{-1}, while the corresponding Sn-free alloy has an activation energy of only 399.84 kJ mol^{-1} [51]. This fact suggests that further optimization in the composition of the $Ti_{30}Zr_{32}Ag_7Pd_{24}Sn_7$ should consider preservation or even an increase in Sn content for higher thermal stability.

Future researches could also consider some additions with small proportions of Sc, Hf, Ta or Nb for augmentation of activation energy. Each of these elements is responsible for increasing the activation energies of the primary crystallization reaction if added initially to $Ti_{53}Cu_{27}Ni_{12}Zr_3Al_7Si_3B_1$ BMG. The most spectacular effect belongs to Cu, Nb and Ta [52]. This fact could also explain the high thermal stability of $Ti_{42}Zr_{40}Ta_3Si_{15}$ that was previously developed [27].

It is worth emphasizing that although the Kissinger's method is subject to some critiques [43], it remains the most used method for calculation of activation energies for crystallization, and comparative studies on glassy Ti alloys evidenced good agreement with other method based on isochronal or isothermal investigations. For example, activation energy for crystallization of $Ti_{48}Ni_{32}Cu_8Si_8Sn_4$ was determined at 369.1 kJ mol^{-1} after Kissinger for isochronal heating and 381.8 kJ mol^{-1} following isothermal methods [53]. The Kissinger's method also gives activation energies of 392 and 320 kJ mol^{-1} for the crystallization reactions of $Ti_{20}Zr_{20}Cu_{60}$ metallic glass, which are very close to the values resulting from alternative non-isothermal methods like Augis–Bennet, Boswell, Ozawa or Gao-Wang [54, 55]. Studies on other BMGs also confirm the good accordance between Kissinger's calculations and the methods of Augis or Moynihan [56].

Conclusions

Microstructural investigation by means of XRD and HR-TEM clearly proves the possibility to cast fully amorphous ribbons of $Ti_{30}Zr_{32}Ag_7Pd_{24}Sn_7$ alloy by means of melt spinning technique despite the reduced glass-forming ability. The newly formulated composition is free of elements like Cu, Ni, Be and Al that are usually used for amorphization of Ti, which are harmful to the human body. The new alloy could also benefit in biomedical applications from the bactericidal effects of the Ag addition, with the condition of in vivo assessment of biocompatibility.

The activation energy calculated after Kissinger's method evidenced values that are in the lowest range reported for the amorphous Ti-based alloys; therefore, a rather low thermal stability is to be expected for the thermomechanical processing. Consequently, the powder metallurgy processing of $Ti_{30}Zr_{32}Ag_7Pd_{24}Sn_7$ ribbons for the fabrication of massive amorphous components should be carried out with precaution to prevent alterations of amorphous character and relevant properties. In comparison with the $Ti_{42}Zr_{40}Ta_3Si_{15}$ that was previously developed and could be successfully consolidated by hot pressing at 550 °C for 3 min, processing should be performed at lower temperature. Thermal processing $Ti_{30}Zr_{32}Ag_7Pd_{24}Sn_7$ ribbons should be pursued below crystallization point that was determined around 500 °C for processing cycles as short as possible. However, literature researches reveal that additive manufacturing techniques could also be applied, which enlarges the technological possibilities for components of intricate shapes, such as scaffolds for biomedical applications. For example, selective laser melting (SLM) allows fabrication of large, complex components of BMGs from amorphous powders, if suitable parameters are used to avoid crystallization [57, 58]. An optimized combination of laser power, laser spot size and dwelling time could guarantee localized melting and subsequent glass formation, even for alloys with moderate GFA. Another research direction that could be explored is further optimization of composition with addition of elements that could improve thermal stability, such as Nb and Ta.

Acknowledgements This work was supported by the German Academic Exchange Service (Deutscher Akademischer Austausch Dienst—DAAD).

References

1. Geetha M, Singh A, Asokamani R, Gogia A. Ti based biomaterials, the ultimate choice for orthopaedic implants—a review. Prog Mater Sci. 2009;54:397–425.
2. Abdel-Hady MG, Niinomi M. Biocompatibility of Ti-alloys for long-term implantation. J Mech Behav Biomed Mater. 2013;20:407–15.
3. Basu B, Katti DS, Kumar A. Advanced biomaterials—fundamentals, processing, and applications. Hoboken: Wiley; 2009.
4. Chen Q, Thouas GA. Metallic implant biomaterials. Mat Sci Eng R. 2015;87:1–57.
5. Biesiekierski A, Wang J, Gepreel MA-H, Wen C. A new look at biomedical Ti-based shape memory alloys. Acta Biomater. 2012;8:1661–9.
6. Inoue A, Takeuchi A. Recent development and application products of bulk glassy alloys. Acta Mater. 2011;59:2243–67.
7. Eckert J, Das J, Pauly S, Duhamel C. Mechanical properties of bulk metallic glasses and composites. J Mater Res. 2007;22(2):285–301.
8. Greer AL. Metallic glasses… on the threshold. Mater Today. 2009;12(1–2):14–23.
9. Oak JJ, Inoue A. Formation, mechanical properties and corrosion resistance of Ti–Pd base glassy alloys. J Non Cryst Solids. 2008;354:1828–32.
10. Yavari A, Lewandowski J, Eckert J. Mechanical properties of bulk metallic glasses. MRS Bull. 2007;32:635–8.
11. Hornez J, Lefevre A, Joly D, Hildebrand H. Multiple parameter cytotoxicity index on dental alloys and pure metals. Biomol Eng. 2002;19:103–17.
12. Elshahawy WM, Watanabe I, Kramer P. In vitro cytotoxicity evaluation of elemental ions released from different prosthodontic materials. Dent Mater. 2009;25:1551–5.
13. Calin M, Gebert A, Ghinea AC, Gostin PF, Abdi S, Mickel C, Eckert J. Designing biocompatible Ti-based metallic glasses for implant applications. Mater Sci Eng C. 2013;33:875–83.
14. Inoue A, Kong F, Zhu S, Shalaan E, Al-Marzouki F. Production methods and properties of engineering glassy alloys and composites. Intermetallics. 2015;58:20–30.
15. Ke J, Huang C, Chen Y, Tsai W, Wei T, Huang J. In vitro biocompatibility response of Ti–Zr–Si thin film metallic glasses. Appl Surf Sci. 2014;322:41–6.
16. Abdi S, Khoshkhoo MS, Shuleshova O, Bönisch M, Calin M, Baró M, Sort J, Gebert A. Effect of Nb addition on microstructure evolution and nanomechanical properties of a glass-forming TiZrSi alloy. Intermetallics. 2014;46:156–63.
17. Lin H, Tsai P, Ke J, Li J, Jang J, Huang C, Haung J. Designing a toxic-element-free Ti-based amorphous alloy with remarkable supercooled liquid region for biomedical application. Intermetallics. 2014;55:22–7.
18. Lin C, Huang C, Chuang J, Huang J, Jang J, Chen C. Rapid screening of potential metallic glasses for biomedical applications. Mater Sci Eng C. 2013;33:4520–6.
19. Zhuravleva K, Chivu A, Teresiak A, Scudino S, Calin M, Schultz L, Eckert J. Porous low modulus $Ti_{40}Nb$ compacts with electrodeposited hydroxyapatite coating for biomedical applications. Mater Sci Eng C. 2013;33:2280–7.
20. Li J, Lin H, Jang JKC, Huang J. Novel open-cell bulk metallic glass foams with promising characteristics. Mater Lett. 2013;105:140–3.
21. Karageorgiou V, Kaplan D. Porosity of 3D biomaterial scaffolds and osteogenesis. Biomaterials. 2005;26:5474–91.
22. Xue W, Krishna BV, Bandyopadhyay A, Bose S. Processing and biocompatibility evaluation of laser processed porous titanium. Acta Biomater. 2007;3:1007–18.
23. Wen C, Yamada Y, Hodgson P. Fabrication of novel TiZr alloy foams for biomedical applications. Mater Sci Eng C. 2006;26:1439–44.
24. Raduta A, Nicoara M, Locovei C, Eckert J, Stoica M. Ti-based bulk glassy composites obtained by replacement of Ni with Ga. Intermetallics. 2016;69:28–34.
25. Nicoara M, Locovei C, Serban VA, Parthiban R, Calin M, Stoica M. New Cu-free Ti-based composites with residual amorphous matrix. Materials. 2016;331:1–14.
26. Nicoara M, Raduta A, Parthiban R, Locovei C, Eckert J, Stoica M. Low Young's modulus Ti-based porous bulk glassy alloy without cytotoxic elements. Acta Biomater. 2016;331:1–14.
27. Nicoara M, Raduta A, Locovei C, Buzdugan D, Stoica M. About thermostability of biocompatible Ti–Zr–Ta–Si amorphous alloys. J Therm Anal Calorim. 2017;127:107–13.
28. Oak JJ, Louzguine-Luzgin DV, Inoue A. Fabrication of Ni-free Ti-based bulk-metallic glassy alloy having potential for application as biomaterial, and investigation of its mechanical properties, corrosion, and crystallization behavior. J Mater Res. 2007;22:1346–53.
29. Stohs S, Bagchi D. Oxidative mechanisms in the toxicity of metal ions. Free Radic Bio Med. 1995;18:321–36.
30. Wataha J, Lockwood P, Schedle A. Effect of silver, copper, mercury, and nickel ions on cellular proliferation during extended, low-dose exposures. J Biomed Mater Res. 2000;52:360–4.
31. Craig R, Hanks C. Cytotoxicity of experimental casting alloys evaluated by cell culture tests. J Dent Res. 1990;69:1539–42.
32. Secinti KD, Özalp H, Attar A, Sargon MF. Nanoparticle silver ion coatings inhibit biofilm formation on titanium implants. J Clin Neurosci. 2011;18:391–5.
33. Choi O, Yu CP, Fernandez GE, Hua Z. Interactions of nanosilver with Escherichia coli cells in planktonic and biofilm cultures. Water Res. 2010;44:6095–103.
34. Kalishwaralal K, BarathManiKanth S, Pandian SRK, Deepak V, Gurunathan S. Silver nanoparticles impede the biofilm formation by *Pseudomonas aeruginosa* and *Staphylococcus epidermidis*. Colloid Surf B. 2010;79:340–4.
35. Abdel-Hady M, Hinoshita K, Morinaga M. General approach to phase stability and elastic properties of beta-type Ti-alloys using electronic parameters. Scr Mater. 2006;55:477–80.
36. Oak JJ, Louzguine-Luzgin DV, Inoue A. Synthetic relationship between titanium and alloying elements in designing Ni-free Ti-based bulk metallic glass alloys. Appl Phys Lett. 2007;91:1–4.
37. Ashby M, Greer A. Metallic glasses as structural materials. Scr Mater. 2006;54:321–6.
38. Suryanarayana C, Inoue A. Bulk metallic glasses. Boca Raton: CRC Press; 2011.
39. Kissinger HE. Reaction kinetics in differential thermal analysis. Anal Chem. 1957;21:1702–6.
40. Srivastava AP, Srivastava D, Mazumdar B, Dey GK. Thermo-analytical study of crystallization process in metallic glass of Co69Fe3Si18B10. J Therm Anal Calorim. 2015;119:1353–61.
41. Strbac G, Strbac D, Lukic-Petrovic S, Siljegovic M. Thermal characterization of glasses from Fe–Sb–S–I system. J Therm Anal Calorim. 2017;127:247–54.
42. Svoboda R, Malek J. Amorphous-to-crystalline transition in Te-doped $Ge_2Sb_2Se_5$ glass. J Therm Anal Calorim. 2014;117:1073–83.
43. Svoboda R, Malek J. Is the original Kissinger equation obsolete today? J Therm Anal Calorim. 2014;115:1961–7.
44. Wu J, Pan Y, Pi J. On non-isothermal kinetics of two Cu-based bulk metallic glasses. J Therm Anal Calorim. 2014;115:267–74.
45. Wei HD, Bao QH, Wang CX, Zhang WS, Yuan ZZ, Chen XD. Crystallization kinetics of $(Ni_{0.75}Fe_{0.25})_{78}Si_{10}B_{12}$ amorphous alloy. J Non Cryst Solids. 2008;354:1876–82.

46. Zhang J, Wang W, Ma H, Li G, Lia R, Zhang Z. Isochronal and isothermal crystallization kinetics of amorphous Fe-based alloys. Thermochim Acta. 2010;505:41–6.
47. Gong P, Wang X, Yao K. Effects of alloying elements on crystallization kinetics of Ti–Zr–Be bulk metallic glass. J Mater Sci. 2016;51:5321–9.
48. Pratap A, Rao TLS, Lad KN, Dhurandhar HD. Kinetics of crystallization of titanium based binary and ternary amorphous alloys. J Non Cryst Solids. 2007;353:2346–9.
49. Zhu SL, Wang XM, Qin FX, Yoshimura M, Inoue A. New TiZrCuPd quaternary bulk glassy alloys with potential of biomedical applications. Mater Trans JIM. 2007;48(9):2445–8.
50. Gong P, Yao K, Zhao S. Cu-alloying effect on crystallization kinetics of $Ti_{41}Zr_{25}Be_{28}Fe_6$ bulk metallic glass. J Therm Anal Calorim. 2015;121:697–704.
51. Huang Y, Shen J, Sun J, Yu X. A new Ti–Zr–Hf–Cu–Ni–Si–Sn bulk amorphous alloy with high glass-forming ability. J Alloy Compd. 2007;427(1–2):171–5.
52. Xia MX, Zheng HX, Jian L, Ma CL, Li JG. Thermal stability and glass-forming ability of new Ti-based bulk metallic glasses. J Non Cryst Solids. 2005;351:3747–51.
53. Khalifa HE, Vecchio KS. Thermal stability and crystallization phenomena of low cost Ti-based bulk metallic glass. J Non Cryst Solids. 2011;357:3393–8.
54. Kasyap S, Patel AT, Pratap A. Crystallization kinetics of $Ti_{20}Zr_{20}Cu_{60}$ metallic glass by isoconversional methods using modulated differential scanning calorimetry. J Therm Anal Calorim. 2014;116:1325–36.
55. Haratian S, Haddad-Sabzevar M. Thermal stability and non-isothermal crystallization kinetics of $Ti_{41.5}Cu_{42.5}Ni_{7.5}Zr_{2.5}Hf_5Si_1$ bulk metallic glass. J Non Cryst Solids. 2015;429:164–70.
56. Lu XC, Li HY. Kinetics of non-isothermal crystallization in $Cu_{50}Zr_{43}Al_7$ and $(Cu_{50}Zr_{43}Al_7)_{95}Be_5$ metallic glasses. J Therm Anal Calorim. 2014;115:1089–97.
57. Li XP, Roberts MP, O'Keeffe S, Sercombe TB. Selective laser melting of Zr-based bulk metallic glasses: processing, microstructure and mechanical properties. Mater Des. 2016;112:217–26.
58. Pauly S, Lober L, Petters R, Stoica M, Scudino S, Kuhn U, Eckert J. Processing metallic glasses by selective laser melting. Mater Today. 2013;16:37–41.